Photonic Gauge Potential in One Cavity with Synthetic Frequency and Orbital Angular Momentum Dimensions

Luqi Yuan, Qian Lin, Anwei Zhang, Meng Xiao, Xianfeng Chen, and Shanhui Fan

Phys. Rev. Lett. **122**, 083903 — Published 1 March 2019

DOI: 10.1103/PhysRevLett.122.083903

Photonic gauge potential in one cavity with synthetic frequency and orbital angular momentum dimensions

Luqi Yuan[1,*], Qian Lin[2], Anwei Zhang[1], Meng Xiao[3], Xianfeng Chen[1,†], and Shanhui Fan[3,‡]

[1] *School of Physics and Astronomy, Shanghai Jiao Tong University, Shanghai 200240, China*

[2] *Department of Applied Physics, Stanford University, Stanford, CA 94305, USA*

[3] *Department of Electrical Engineering, and Ginzton Laboratory, Stanford University, Stanford, CA 94305, USA*

[*] *Corresponding author: yuanluqi@sjtu.edu.cn*

[†] *Corresponding author: xfchen@sjtu.edu.cn*

[‡] *Corresponding author: shanhui@stanford.edu*

(Dated: February 5, 2019)

Abstract

We explore a single degenerate optical cavity supporting a synthetic two dimensional space, which includes the *frequency* and the *orbital angular momentum* axes of light. We create the effective gauge potential inside this synthetic space and show that the system exhibits topologically-protected one-way edge states along the OAM axis at the boundaries of the frequency dimension. In this synthetic space, we present a robust generation and manipulation of entanglement between the frequency and OAM of photons. Our work shows that a higher dimensional synthetic space involving multiple degrees of freedom of light can be achieved in a "zero" dimensional spatial structure, pointing towards a unique platform to explore topological photonics and to realize potential applications in optical communications and quantum information processing.

The synthetic dimension in photonics has been explored with great interest in the past few years [1–6]. Various degrees of freedom of photons, such as their frequency [5–14] and their orbital angular momentum (OAM) [4, 15–18], have been used to construct the synthetic space. By combining the spatial dimension with either the frequency or the OAM dimension, one can use a one-dimensional array of optical cavities to create a two-dimensional synthetic space [4–6]. In such synthetic spaces, it is possible to explore various high dimensional physics effects with a low dimensional physical structure, including photonic gauge potential [4–6], topological photonics [8, 9, 12, 16, 17], and photonic physics with parity-time symmetry [13]. Furthermore, these constructions enable not only the control of light propagation along the spatial dimension, but also the manipulation of either the frequency or the OAM of light. Such capabilities lead to various potential applications in the fields of optical communications and quantum information processing [1, 19–24].

In most previous proposals towards two or higher dimensional systems with one of the dimensions being a synthetic dimension, the spatial dimension is still required in terms of the use of multiple cavities [4–6, 8, 9, 14–16]. The use of multiple cavities adds significant complexity to experimental implementations. For example, in multi-cavity systems one needs to align all resonant frequencies in each cavity with respect to one another. In this article, we show that it is possible to achieve a two-dimensional synthetic space with only one single degenerate optical cavity. The synthetic space is composed of one *frequency* dimension and one *orbital angular momentum* dimension of light. No spatial dimension is required.

We also propose to create a photonic gauge potential in such a synthetic space. The concept of an effective gauge potential for photons was first proposed in real space, and it provides new capabilities in controlling the spatial flow of light [25–28, 31–33]. One important consequence of the photonic gauge potential is the creation of an effective magnetic field for photons [25, 27, 28]. Such effective magnetic field breaks time-reversal symmetry and creates topologically protected one-way edge states, which is robust to variation of system details [29, 30]. The photonic gauge potential can also be implemented in a synthetic space with an array of cavities [4, 5]. We explore the effective gauge potential in the synthetic space in our proposal. A secondary cavity is used to create artificial frequency boundaries. The frequency of a resonant mode in the secondary cavity is aligned with one resonant mode in the main cavity, so it provides a hard cutoff at the corresponding frequency. Topologically-protected one-way edge states are found to be located at the boundaries in the frequency

dimension and propagating unidirectionally along the OAM axis. Because of the connectivity between the frequency and OAM axes, one can achieve a topologically-protected manipulation of entangled photon states. Our work creates a synthetic space including more than one degree of freedom of light in a "zero" dimensional spatial structure, which provides a unique platform to explore the photonic gauge potential and to manipulate the quantum state of light which is potentially important for quantum optical communication.

We start by considering a single degenerate optical ring cavity shown in Fig. 1(a). The optical elements are chosen to have cylindrical symmetry, so the transverse profile of the cavity modes are the Laguerre-Gaussian modes [4, 34]. In such a degenerate cavity, the resonant frequency is independent of the radial and azimuthal mode index of the transverse modal profile [35–37]. Hence it supports a set of resonant modes with frequencies $\omega_n = \omega_0 + n\Omega$. Here ω_0 is the frequency for the 0th mode, n is an integer, and $\Omega = 2\pi c/L \ll \omega_0$ is the free-spectral-range of the optical cavity, where L is the length of the cavity.

We can expand the electric field E in the degenerate optical cavity as $E = \sum_{l,n} c_{l,n} A_{l,n}(r_\perp) e^{i(k_n z - \omega_n t)} e^{-il\phi}$, where $A_{l,n}$ is the modal profile along the radial dimension $r_\perp$ perpendicular to the circulating beam [4, 5, 38]. $c_{l,n}$ is the modal amplitude for the eigenmode at the frequency ω_n and the OAM l. $k_n = \omega_n/c$ is the wavevector for the modes with frequency ω_n, and z denotes the propagation axis for the circulating beam. l, which is an integer, denotes the angular momentum of the circulating beam. ϕ denotes the azimuthal coordinate.

The cavity shown in Fig. 1(a) consists of a main loop and an auxiliary path. We place an electro-optic phase modulator (EOM) inside the main loop of the cavity. The modulation has a time-dependent transmission coefficient $T = e^{i2\beta\cos(\Omega_M t)}$, where Ω_M is the modulation frequency and β denotes the modulation amplitude. We consider the weak modulation regime with the modulation strength $g \equiv \beta\Omega/2\pi \ll \Omega$. The change of the modal amplitude after each round trip due to passing through the EOM gives

$$\frac{d}{dt} c_{l,n} = ig(c_{l,n+1} e^{i\Delta t} + c_{l,n-1} e^{-i\Delta t}), \tag{1}$$

where $\Delta = \Omega_M - \Omega \ll \Omega$ is the detuning of the modulation frequency from the free spectral range of the cavity.

A pair of beam splitters [at positions A and H in Fig. 1(a)] is placed in the main loop of the optical cavity to divert a small portion of light into an auxiliary path. Inside this

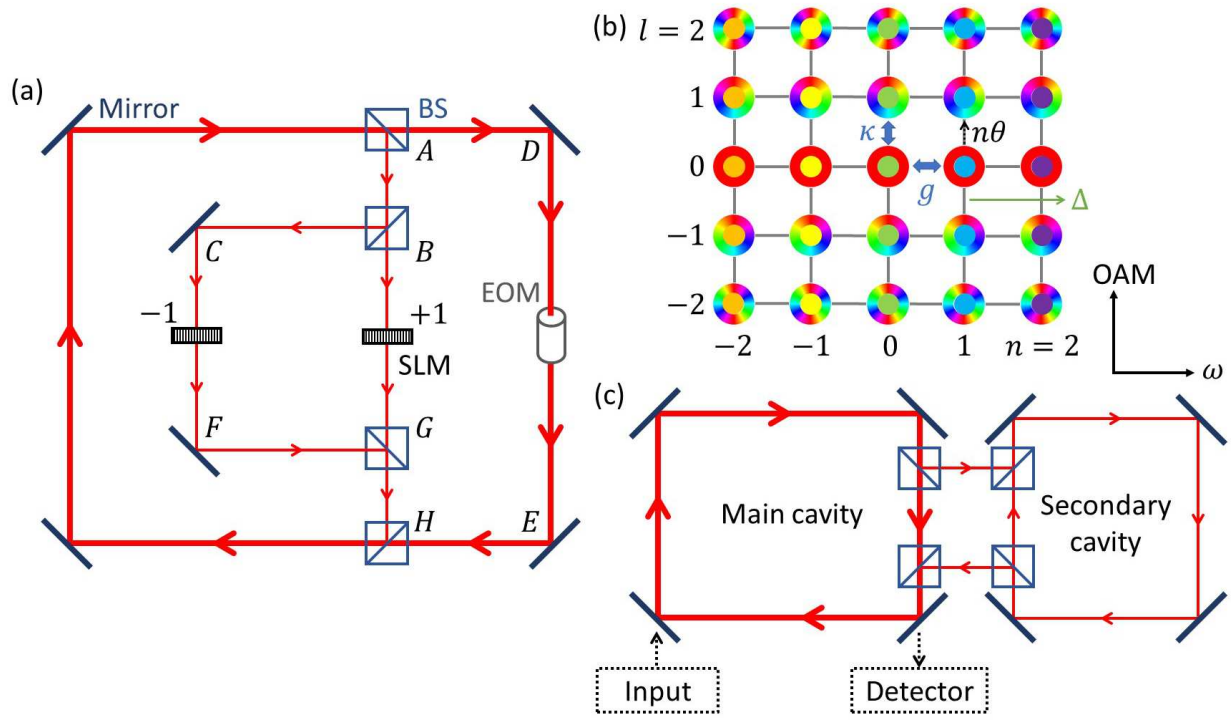

FIG. 1: (a) A single optical cavity including an auxiliary path, which is split into two arms $A \to B \to G \to H$ and $A \to B \to C \to F \to G \to H$. EOM denotes the electro-optic phase modulator, SLM is the spatial light modulator, and BS is the beam splitter. (b) A synthetic two-dimensional space consisted of the frequency and OAM axes of light. (c) A secondary cavity is coupled to the main cavity to provide the artificial boundaries in the frequency dimension. Input/output channel to the main cavity is created by changing the transmissivity/reflectivity of mirrors.

auxiliary path, light is split equally into two separate arms. Each arm has a spatial light modulator (SLM), which changes the OAM of light by either $+1$ or -1. Here bandwidths of two SLMs are assumed to be much larger than Ω, so SLMs perform same operations for all ω_n. The lengths of the two arms between positions A and H are set to be different, i.e., we choose $L_{A\to B\to G\to H} - L_{A\to D\to E\to H} = L_{A\to D\to E\to H} - L_{A\to B\to C\to F\to G\to H} = \delta L$. For light at a frequency ω_n, the difference in propagation phase due to such a mismatch in arm lengths is $k_n \delta l = \omega_0 \delta l/c + n\Omega\delta l/c \equiv \theta_0 + n\theta$, which is dependent on n (i.e. the resonant frequency ω_n). For our purpose here, θ_0 is a global phase, which can be neglected without loss of generality. We further require that there is no resonant loop except for the main loop in the optical cavity, so we set $\theta/2\pi \equiv \Omega\delta l/2\pi c$ to be an irrational number. Therefore, this auxiliary path

contributes to a change of the modal amplitude after each round trip as

$$\frac{d}{dt}c_{l,n} = i\kappa(c_{l+1,n}e^{in\theta} + c_{l-1,n}e^{-in\theta}), \tag{2}$$

where $\kappa \ll \Omega$ denotes the rate for the change between two nearest-neighbor OAMs after the field passes through the auxiliary path.

Thus the system in Fig. 1(a) can be described by the Hamiltonian

$$H = \sum_{l,n} g(a^{\dagger}_{l,n+1}a_{l,n}e^{i\Delta t} + a^{\dagger}_{l,n-1}a_{l,n}e^{-i\Delta t}) + \kappa(a^{\dagger}_{l+1,n}a_{l,n}e^{in\theta} + a^{\dagger}_{l-1,n}a_{l,n}e^{-in\theta}), \tag{3}$$

here we set $\hbar = 1$. $a_{l,n}$ ($a^{\dagger}_{l,n}$) is the annihilation (creation) operator for the mode at the frequency ω_n and the OAM l. We use $a_{l,n} = b_{l,n}e^{in\Delta t}$ and transform the Hamiltonian in Eq. (3) to

$$\tilde{H} = \sum_{n} n\Delta b^{\dagger}_{l,n}b_{l,n} + g(b^{\dagger}_{l,n+1}b_{l,n} + b^{\dagger}_{l,n-1}b_{l,n}) + \kappa(b^{\dagger}_{l+1,n}b_{l,n}e^{in\theta} + b^{\dagger}_{l-1,n}b_{l,n}e^{-in\theta}). \tag{4}$$

Eq. (4) presents a two dimensional synthetic space defined by the frequency and the OAM axes of light [see Fig. 1(b)]. The distribution of hopping phases follows the Landau gauge and generates a uniform magnetic flux θ in each unit cell. The modulation detuning Δ gives an effective electric field along the synthetic frequency dimension. One can therefore manipulate both the OAM and the frequency of light simultaneously in this synthetic space by controlling the effective electric and magnetic fields for light.

We first explore the topological effect due to the presence of the effective magnetic field in the synthetic space. For this purpose, we set $\Delta = 0$ and $\kappa = g$. The eigenspectrum of the Hamiltonian (4) exhibits the *Hofstadter butterfly* pattern [39], as shown in Fig. 2(a), where we plot the eigenspectrum with different θ. ε, the eigenvalue, is obtained by diagonalizing Eq. (4). An input optical field with the frequency shift ε regarding to an arbitrary ω_n may excite a propagating mode in the synthetic space for the system, provided that ε lies outside the band gap [4–6]. In our design, θ is related to δL and can be tuned by changing the lengths of two arms. We restrict $\delta L < L$ so that $\theta/2\pi < 1$. We plot the eigenspectrum up to $\theta/2\pi = 0.8$, where the design of the cavity is physically feasible.

In our setup, θ can be continuously tuned and therefore can assume any number. Thus, one can realize an effective magnetic field incommensurate with the lattice. As an illustration, we choose $\theta/2\pi = \left(\sqrt{5}-1\right)/2$ [which corresponds to the red line in Fig. 2(a)]. For this

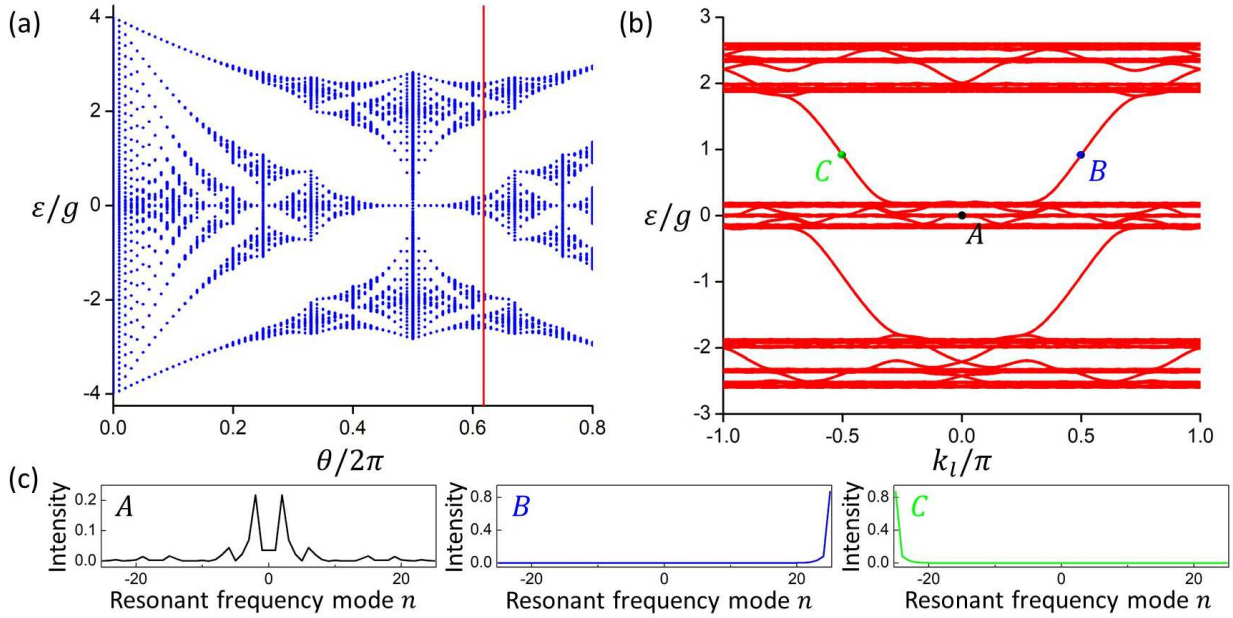

FIG. 2: (a) Projected eigenspectrum versus θ from the Hamiltonian (4). $\Delta = 0$ and $\kappa = g$. (b) Projected eigenspectrum with $\theta/2\pi = \left(\sqrt{5}-1\right)/2$, indicated by the red line in (a). 51 resonant frequency modes are considered. k_l is the wavevector reciprocal to the synthetic OAM dimension. (c) The corresponding eigenstates for the field intensity at $(k_l/\pi, \varepsilon/g) = (0, 0)$ (Black), $(0.5, 0.9)$ (Blue), and $(-0.5, 0.9)$ (Green) labelled in (a), respectively.

system, the Hamiltonian of Eq. (4) is still periodic along the OAM axis. Therefore, we plot the projected bandstructure versus k_l, which is the wavevector reciprocal to the synthetic OAM axis of light in Fig. 2(b). We choose 51 resonant frequency modes ($\omega_n \in [\omega_{-25}, \omega_{25}]$) and assume a boundary along the frequency axis. (We will discuss how such a boundary can be created in the detailed simulation below). The effective magnetic flux θ breaks the time-reversal symmetry in the synthetic space, and makes the system topologically non-trivial. One can see that, near $\varepsilon/g \sim 1$, the bandgap is open and there are two pairs of topologically-protected one-way edge modes inside the gap. The edge modes are strongly localized at the boundary along the frequency axis, whereas the bulk modes are delocalized throughout the synthetic space [see Fig. 2(c)].

We then perform the simulation to observe the evolutions of edge states in the synthetic space. To create the artificial boundaries in the frequency dimension, we couple the optical cavity with a secondary cavity as shown in Fig. 1(c), which is designed to be resonant with the frequency $\omega_{\pm(N+1)}$ (where N is a large positive integer), but to be off resonant with all

other frequencies in-between, i.e. $\omega_n \in [\omega_{-N}, \omega_N]$. Such a secondary cavity then creates artificial boundaries at $\omega_{\pm N}$. Input/output channels are also introduced so that one can inject light into and extract light out from the main cavity. The coupled-mode equations for this system read [38, 40, 41]

$$\frac{dc_{l,n}}{dt} = -\gamma c_{l,n} - ig\left(c_{l,n-1} + c_{l,n+1}\right) - ig\left(c_{l-1,n}e^{in\theta} + c_{l+1,n}e^{-in\theta}\right)$$

$$-i\eta f_{l,N+1}\delta_{n,N+1} - i\eta f_{l,-(N+1)}\delta_{n,-(N+1)} + \sqrt{\gamma}s^{\text{in}}_{l,n}, \tag{5}$$

$$\frac{df_{l,\pm(N+1)}}{dt} = -i\eta c_{l,\pm(N+1)}, \tag{6}$$

$$s^{\text{out}}_{l,n} = \sqrt{\gamma}c_{l,n}. \tag{7}$$

Here η is the coupling constant between the main cavity and the secondary cavity. $\gamma/2$ is the decay rate through the coupling between the main cavity and the input/output channel. $f_{l,n}$ and $s^{\text{in}}_{l,n}$ ($s^{\text{out}}_{l,n}$) are the modal amplitudes for the mode in the secondary cavity and the input (output) amplitudes, respectively, at the frequency ω_n and OAM l.

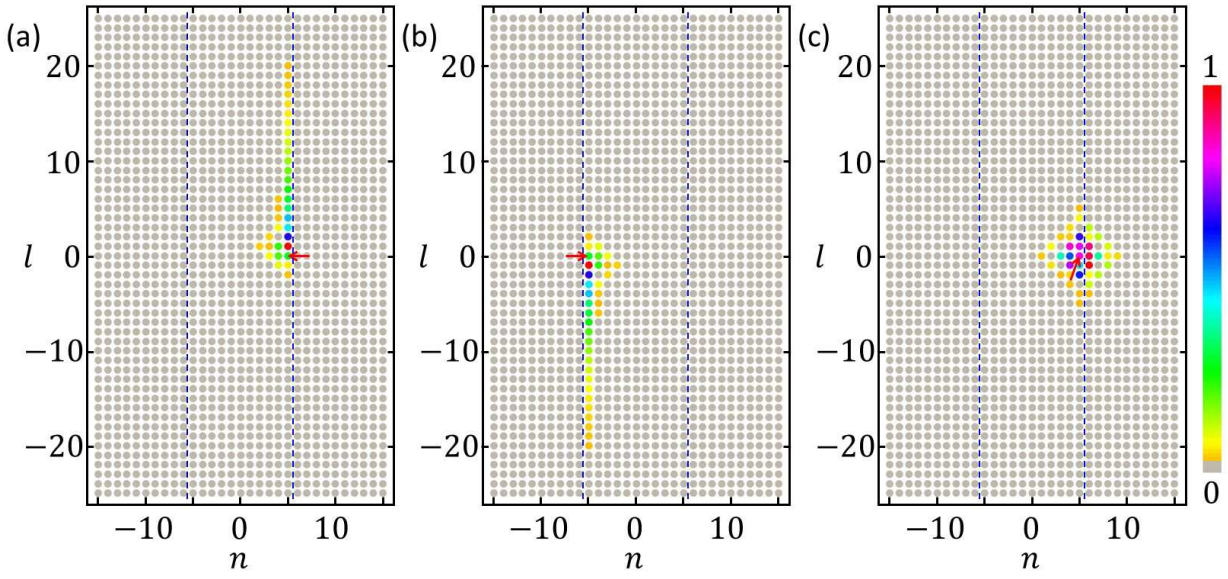

FIG. 3: The steady-state solutions of the normalized intensities $|s^{\text{out}}_{l,n}|^2$ for the output field with the frequency ω_n and the OAM l by solving Eqs. (5)-(7). (a) and (b) $\eta = 10g$, which creates artificial boundaries in the frequency dimension. (c) $\eta = g$, where the artificial boundary is inefficient and no edge state is created. The desired artificial boundaries are labelled by blue dashed line. Red arrows denote modes (n and l) of initial excitations from the input source.

In the simulation, we consider a synthetic space consisting of 31 frequency components ($n = -15 \ldots 15$) and 51 OAM components ($l = -25 \ldots 25$). For the secondary cavity, we set $N = 5$ and vary η to achieve the artificial boundaries at $\omega_{\pm N}$. The input/output channel couples with the main cavity at a rate $\gamma = 0.14g$ and the input source is a monochromatic field with $l = 0$. All other parameters are the same as those in calculating the bandstructure in Fig. 2. In both Figs. 3(a) and 3(b), we plot the steady-state solution for the normalized intensities $|s_{l,n}^{\text{out}}|^2$ in the synthetic space from simulating Eqs. (5)-(7) with $\eta = 10g$. In Fig. 3(a), we set the input source $s_{l,n}^{\text{in}} = \delta_{l,0}\delta_{n,N}e^{-igt}$. In Fig. 3(b), we set $s_{l,n}^{\text{in}} = \delta_{l,0}\delta_{n,-N}e^{-igt}$. The small frequency shift term e^{-igt} is designed to excite the topologically-protected one-way edge mode shown in Fig. 2. We can see the edge modes both in Figs. 3(a) and 3(b). In Fig. 3(a), the edge mode propagates unidirectionally along the positive direction of the synthetic OAM axis, while it propagates along the negative direction in Fig. 3(b). The edge modes are localized at the frequency boundaries of $\omega_{\pm N}$, demonstrating that the artificial boundary along the synthetic frequency axis can be created by introducing a secondary cavity. As a comparison, we also perform the simulation with the same parameters but $\eta = g$ in Fig. 3(c). In this case, the coupling η due to the secondary cavity is weak and the artificial boundary is inefficient. No edge state is created. The amplitudes are instead localized near the source since the frequency is in the bandgap for the bulk. Therefore, one requires a large coupling η to create an artificial boundary in the frequency dimension.

The intrinsic cavity loss γ_i can also be set as a parameter. In the Supplemental Material, we show that one can control the evolution of edge states by changing γ_i [42]. In Fig. 3, there is no boundary along the OAM axis. It is also possible to construct a sharp OAM boundary by following the method proposed in Ref. [17], and hence create a synthetic two dimensional lattice that is finite along both dimensions. The simulation in this square lattice shows the edge state can propagates unidirectionally through the corner of the frequency and OAM edges, which indicates the robustness due to topological protection [42]. The phenomena of the edge states, alternatively, might be described from the perspective of the phase accumulation of a detuned input from the resonance once it circulates after roundtrips. Besides probing the edge states, we can also probe the bulk property of our system, such as the transmission property in the synthetic space, which provides a direct way to measure the eigenspectrum shown in Fig. 2(b) [42].

One potential application of our system is the generation of entangled pair of photons

with different OAMs. Such entangled photon pair is of great importance in the field of optical quantum communication and quantum information processing [19]. Typical method to prepare the entangled photon pair is to use the spontaneous parametric down-conversion, and the generated entangled state is

$$|\Psi^{\pm}\rangle = \frac{1}{\sqrt{2}}\left(|1_{\omega_A}1_{\omega_B}\rangle \pm |1_{\omega_B}1_{\omega_A}\rangle\right), \tag{8}$$

where $1_{\omega_{A(B)}}$ means that one photon is excited at the frequency $\omega_{A(B)}$. Thus the entanglement occurs between photons with different frequencies. In our synthetic space, one can transfer this entanglement to photons with different OAMs, in a fashion that is topologically protected.

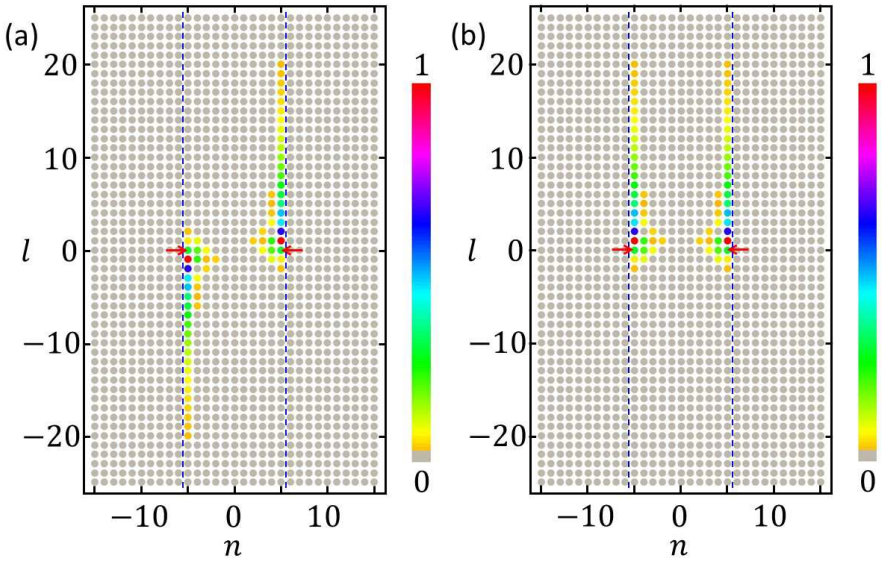

FIG. 4: The steady-state solutions of the normalized intensities $|s^{\text{out}}_{l,n}|^2$ for the output field with the frequency ω_n and the OAM l. (a) The input entangled photon pair in Eq. (8) has the 0-th OAM and frequencies $\omega_A = \omega_{-N} + g$, $\omega_B = \omega_N + g$. (b) The photon pair has $\omega_A = \omega_{-N} - g$, $\omega_B = \omega_N + g$. The desired artificial boundaries are labelled by blue dashed line. Red arrows denote modes (n and l) of initial excitations from the input source.

To demonstrate it, we use the same parameters as those in the simulation of Fig. 3(a). We choose the input entangled photon pair with $\omega_A = \omega_{-N} + g$, $\omega_B = \omega_N + g$, and its OAM $l = 0$. In Fig. 4(a), we plot the simulation result. One see that a pair of edge modes propagate along the positive/negative direction of the OAM axis with the same speed. The two-photon state thus evolves to a new state $|\Psi_1^{\pm}\rangle = \sum_{l\geq 0} \alpha_l \left(|1_{\omega_A,-l}1_{\omega_B,l}\rangle \pm |1_{\omega_B,l}1_{\omega_A,-l}\rangle\right)$, where α_l

represents the transfer coefficient. This state is a multi-dimensional entangled state for two photons, which has fundamental importance in quantum communication [19, 43–45]. For this state, the entanglement exists between photons with opposite OAMs. Alternatively, we can also create state where the entanglement occurs between photons with the same OAM. For this purpose, in Fig. 4(b), we perform the simulation where the initial input photon pair has $\omega_A = \omega_{-N} - g$ and $\omega_B = \omega_N + g$. In this case, the edge modes that are excited both propagate along the positive OAM axis. The generated new state becomes $|\Psi_2^{\pm}\rangle = \sum_{l\geq 0} \alpha_l \left(|1_{\omega_A,l} 1_{\omega_B,l}\rangle \pm |1_{\omega_B,l} 1_{\omega_A,l}\rangle\right)$. The transfer between the frequency entanglement and OAM entanglement is a robust process due to the topological protection, providing the potential application towards the quantum entanglement of two different degrees of freedom of photons, which is of fundamental importance in quantum optics [46].

To implement our concept experimentally, we consider free-space optics, which provides many choices for EOMs and SLMs. The operation frequency for the SLM is $\omega_0 \sim 100$ THz. The length of the optical cavity is on the order of 1–10 m, which sets the mode spacing and the modulation frequency of the EOM at $\Omega \sim$10–100 MHz$\ll \omega_0$. This makes the resonant modes being spectrally dense. SLM therefore works fine for resonant modes at frequencies near ω_0. The modulation strength g shall be much smaller than Ω, i.e. $g \sim$0.5–5 MHz, which also makes $\eta < \Omega$. Loss in the cavity includes transmissions through the input/output channels (mirrors), as well as intrinsic losses associated with reflections on mirrors, modulations in the EOM and SLMs, and also travelling through the additional path. One can compensate for the loss and tune γ_i [42] by placing an amplifier in the optical path inside the main cavity, operated with a lower gain without inducing lasing, which dramatically increase the quality factor of the optical cavity [47].

In summary, we propose a two-dimensional synthetic space in a single degenerate optical cavity including the frequency and the OAM axes of light, where the photonic gauge potential can be created. A secondary cavity is used to create artificial boundaries in the synthetic frequency dimension. We show that such a system supports topologically-protected one-way edge states at the boundaries of the frequency dimension propagating unidirectionally along the OAM dimension. Our system hence provides a unique platform to explore two-dimensional topological physics in a "zero" dimensional spatial structure. Compared with previous works that use a one-dimensional array of cavities to simulate two dimensional physics [1, 4–6], our system here is easier to implement, since there is no longer a need to align

the resonances of multiple cavities. Moreover, our system provides a connection between the OAM and the frequency of photons. With this connection, one can demonstrate a topologically-protected manipulation of entangled photon states, which is potentially useful for applications in quantum optical communications.

Acknowledgments

The authors acknowledge stimulating discussions with Dr. Avik Dutt. This paper is supported by the National Key R&D Program of China (2018YFA0306301 and 2017YFA0303701). This paper is also partially supported by the U.S. Air Force Office of Scientific Research Grants No FA9550-17-1-0002, as well as the U.S. National Science Foundation Grant No. CBET-1641069.

---

[1] L. Yuan, Q. Lin, M. Xiao, and S. Fan, "Synthetic Dimension in Photonics," Optica **5**, 1396 (2018).

[2] A. Regensburger, C. Bersch, M.-A. Miri, G. Onishchukov, D. N. Christodoulides, and U. Peschel, "Parity-time synthetic photonic lattices," Nature **488**, 167–171 (2012).

[3] A. Schwartz and B. Fischer, "Laser mode hyper-combs," Opt. Express **21**, 6196–6204 (2013).

[4] X.-W. Luo, X. Zhou, C.-F. Li, J.-S. Xu, G.-C. Guo, and Z.-W. Zhou, "Quantum simulation of 2D topological physics in a 1D array of optical cavities," Nat. Commun. **6**, 7704 (2015).

[5] L. Yuan, Y. Shi, and S. Fan, "Photonic gauge potential in a system with a synthetic frequency dimension," Opt. Lett. **41**, 741–744 (2016).

[6] T. Ozawa, H. M. Price, N. Goldman, O. Zilberberg, and I. Carusotto, "Synthetic dimensions in integrated photonics: From optical isolation to four-dimensional quantum Hall physics," Phys. Rev. A **93**, 043827 (2016).

[7] L. Yuan and S. Fan, "Bloch oscillation and unidirectional translation of frequency in a dynamically modulated ring resonator," Optica **3**, 1014–1018 (2016).

[8] Q. Lin, M. Xiao, L. Yuan, and S. Fan, "Photonic Weyl point in a two-dimensional resonator lattice with a synthetic frequency dimension," Nat. Commun. **7**, 13731 (2016).

[9] Y. Zhang and Y. Zhu, "Generation of Weyl points in coupled optical microdisk-resonator

arrays via external modulation," Phys. Rev. A **96**, 013811 (2017).

[10] B. A. Bell, K. Wang, A. S. Solntsev, D. N. Neshev, A. A. Sukhorukov, and B. J. Eggleton, "Spectral photonic lattices with complex long-range coupling," Optica **4**, 1433–1436 (2017).

[11] C. Qin, F. Zhou, Y. Peng, D. Sounas, X. Zhu, B. Wang, J. Dong, X. Zhang, A. Alù, and P. Lu, "Spectrum control through discrete frequency diffraction in the presence of photonic gauge potentials," Phys. Rev. Lett. **120**, 133901 (2018).

[12] L. Yuan, M. Xiao, Q. Lin, and S. Fan, "Synthetic space with arbitrary dimensions in a few rings undergoing dynamic modulation," Phys. Rev. B **97**, 104105 (2018).

[13] L. Yuan, Q. Lin, M. Xiao, A. Dutt, and S. Fan, "Pulse shortening in an actively mode-locked laser with parity-time symmetry," APL Photonics **3**, 086103 (2018).

[14] Q. Lin, X.-Q. Sun, M. Xiao, S.-C. Zhang, and S. Fan, "A three-dimensional photonic topological insulator using a two-dimensional ring resonator lattice with a synthetic frequency dimension," Sci. Adv. **4**, eaat2774 (2018).

[15] X.-W. Luo, X. Zhou, J.-S. Xu, C.-F. Li, G.-C. Guo, C. Zhang, and Z.-W. Zhou, "Synthetic-lattice enabled all-optical devices based on orbital angular momentum of light," Nat. Commun. **8**, 16097 (2017).

[16] B. Y. Sun, X. W. Luo, M. Gong, G. C. Guo, and Z. W. Zhou, "Weyl semimetal phases and implementation in degenerate optical cavities," Phys. Rev. A **96**, 013857 (2017).

[17] X.-F. Zhou, X.-W. Luo, S. Wang, G.-C. Guo, X. Zhou, H. Pu, and Z.-W. Zhou, "Dynamically manipulating topological physics and edge modes in a single degenerate optical cavity," Phys. Rev. Lett. **118**, 083603 (2017).

[18] X.-W. Luo, C. Zhang, G.-C. Guo, and Z.-W. Zhou, "Topological photonic orbital-angular-momentum switch," Phys. Rev. A **97**, 043841 (2018).

[19] A. Mair, A. Vaziri, G. Weihs, and A. Zeilinger, "Entanglement of the orbital angular momentum states of photons," Nature **412**, 313–316 (2001).

[20] J. Wang, J.-Y. Yang, I. M. Fazal, N. Ahmed, Y. Yan, H. Huang, Y. Ren, Y. Yue, S. Dolinar, M. Tur, and A. E. Willner, "Terabit free-space data transmission employing orbital angular momentum multiplexing," Nat. Photonics **6** 488–496 (2012).

[21] N. Bozinovic, Y. Yue, Y. Ren, M. Tur, P. Kristensen, H. Huang, A. E. Willner, S. Ramachandran, "Terabit-Scale Orbital Angular Momentum Mode Division Multiplexing in Fibers," Science **340**, 1545 (2013).

[22] M. Mirhosseini, O. S. Magaña-Loaiza, M. N. O'Sullivan, B. Bodenburg, M. Malik, M. P. J. Lavery, M. J. Padgett, D. J. Gauthier, and R. W. Boyd, "High-dimensional quantum cryptography with twisted light," New J. Phys. **17**, 033033 (2015).

[23] D.-S. Ding, W. Zhang, Z.-Y. Zhou, S. Shi, G.-Y. Xiang, X.-S. Wang, Y.-K. Jiang, B.-S. Shi, and G.-C. Guo, "Quantum Storage of Orbital Angular Momentum Entanglement in an Atomic Ensemble," Phys. Rev. Lett. **114**, 050502 (2015).

[24] Z.-Y. Zhou, S.-L. Liu, Y. Li, D.-S. Ding, W. Zhang, S. Shi, M.-X. Dong, B.-S. Shi, and G.-C. Guo, "Orbital Angular Momentum-Entanglement Frequency Transducer," Phys. Rev. Lett. **117**, 103601 (2016).

[25] M. Hafezi, E. A. Demler, M. D. Lukin, and J. M. Taylor, "Robust optical delay lines with topological protection," Nature Phys. **7**, 907–912 (2011).

[26] R. O. Umucalilar and I. Carusotto, "Artificial gauge field for photons in coupled cavity arrays," Phys. Rev. A **84**, 043804 (2011).

[27] K. Fang, Z. Yu, and S. Fan, "Realizing effective magnetic field for photons by controlling the phase of dynamic modulation," Nat. Photonics **6**, 782–787 (2012).

[28] M. Hafezi, S. Mittal, J. Fan, A. Migdall, and J. M. Taylor, "Imaging topological edge states in silicon photonics," Nat. Photonics **7**, 1001–1005 (2013).

[29] L. Lu, J. D. Joannopoulos, and M. Soljačić, "Topological Photonics," Nat. Photonics **8**, 821–829 (2014).

[30] T. Ozawa, H. M. Price, A. Amo, N. Goldman, M. Hafei, L. Lu, M. C. Rechtsman, D. Schuster, J. Simon, O. Zilberberg, and I. Carusotto, "Topological Photonics," arXiv:1802.04173v1 (2018).

[31] K. Fang and S. Fan, "Effective magnetic field for photons based on the magneto-optical effect," Phys. Rev. A **88**, 043847 (2013).

[32] F. Liu and J. Li, "Gauge Field Optics with Anisotropic Media," Phys. Rev. Lett. **114**, 103902 (2015).

[33] L. Yuan and S. Fan, "Three-dimensional dynamic localization of light from a time-dependent effective gauge field for photons," Phys. Rev. Lett. **114**, 243901 (2015).

[34] N. Hodgson and H. Weber, Laser resonators and beam propagation (Springer, New York, 2005).

[35] J. A. Arnaud, "Degenerate optical cavities," Appl. Opt. **8**, 189–195 (1969).

[36] S. Gigan, L. Lopez, N. Treps, A. Maître, and C. Fabre, "Image transmission through a stable paraxial cavity," Phys. Rev. A **72**, 023804 (2005).

[37] B. Chalopin, A. Chiummo, C. Fabre, A. Maître, and N. Treps, "Frequency doubling of low power images using a self-imaging cavity," Opt. Express **18**, 8033 (2010).

[38] H. A. Haus, Waves and Fields in Optoelectronics (Prentice-Hall, 1984).

[39] D. R. Hofstadter, "Energy levels and wave functions of Bloch electrons in rational and irrational magnetic fields," Phys. Rev. B **14**, 2239–2249 (1976).

[40] S. Fan, W. Suh, and J. D. Joannopoulos, "Temporal coupled-mode theory for the Fano resonance in optical resonators," J. Opt. Soc. Am. A **20**, 569 (2003).

[41] M. Minkov, Y. Shi, and S. Fan, "Exact solution to the steady-state dynamics of a periodically modulated resonator," APL Photonics **2**, 076101 (2017).

[42] See Supplemental Material at http://link.aps.org/ supplemental/, which includes simulations of the influence of the intrinsic loss of the cavity, the propagation of the edge state in a synthetic square lattice, and studies of the transmission property of our system.

[43] A. C. Dada, J. Leach, G. S. Buller, M. J. Padgett, and E. Andersson, "Experimental high-dimensional two-photon entanglement and violations of generalized Bell inequalities," Nat. Phys. **7**, 677–680 (2011).

[44] M. Agnew, J. Leach, M. McLaren, F. S. Roux, and R. W. Boyd, "Tomography of the quantum state of photons entangled in high dimensions," Phys. Rev. A **84**, 062101 (2011).

[45] M. Krenn, M. Huber, R. Fickler, R. Lapkiewicz, S. Ramelow, and A. Zeilinger, "Generation and confirmation of a (100×100)-dimensional entangled quantum system," Proc. Natl. Acad. Sci. USA **111**, 6243–6247 (2014).

[46] T. Stav, A. Faerman, E. Maguid, D. Oren, V. Kleiner, E. Hasman, M. Segev, "Quantum entanglement of the spin and orbital angular momentum of photons using metamaterials," **261**, 1101 (2018).

[47] A. Dutt, M. Minkov, Q. Lin, L. Yuan, D. A. B. Miller, S. Fan, "Experimental band structure spectroscopy along the synthetic frequency dimension," under preparation.